Faraday Discussions

Accepted Manuscript

This manuscript will be presented and discussed at a forthcoming Faraday Discussion meeting. All delegates can contribute to the discussion which will be included in the final volume.

Register now to attend! Full details of all upcoming meetings: http://rsc.li/fd-upcoming-meetings

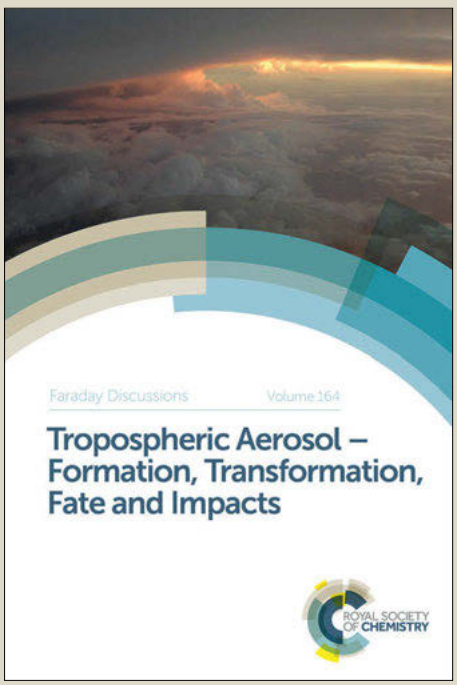

This is an *Accepted Manuscript*, which has been through the Royal Society of Chemistry peer review process and has been accepted for publication.

Accepted Manuscripts are published online shortly after acceptance, before technical editing, formatting and proof reading. Using this free service, authors can make their results available to the community, in citable form, before we publish the edited article. We will replace this *Accepted Manuscript* with the edited and formatted *Advance Article* as soon as it is available.

You can find more information about *Accepted Manuscripts* in the Information for Authors.

Please note that technical editing may introduce minor changes to the text and/or graphics, which may alter content. The journal's standard Terms & Conditions and the Ethical guidelines still apply. In no event shall the Royal Society of Chemistry be held responsible for any errors or omissions in this *Accepted Manuscript* or any consequences arising from the use of any information it contains.

ROYAL SOCIETY OF CHEMISTRY

www.rsc.org/faraday_d

REVIEW www.rsc.org/xxxxxx | XXXXXXXX

Selection, characterisation and mapping of complex electrochemical processes at individual single-walled carbon nanotubes: the case of serotonin oxidation

Aleix G. Güell,[a] Katherine E. Meadows,[a,b] Petr V. Dudin,[a] Neil Ebejer,[a] Joshua C. Byers,[a] Julie V. Macpherson[a] and Patrick R. Unwin[a,*]

DOI: 10.1039/b000000x [DO NOT ALTER/DELETE THIS TEXT]

The electrochemical (EC) oxidation of the neurotransmitter, serotonin, at individual single-walled carbon nanotubes (SWNTs) is investigated at high resolution using a novel platform that combines flow-aligned SWNTs with atomic force microscopy, Raman microscopy, electronic conductance measurements, individual SWNT electrochemistry and high-resolution scanning electrochemical cell microscopy (SECCM). SECCM has been used to visualise the EC activity along side-wall sections of metallic SWNTs to assess the extent to which side-walls promote the electrochemistry of this complex multistep process. Uniform and high EC activity is observed that is consistent with significant reaction at the side-wall, rather than electrochemistry being driven by defects alone. By scanning forward and reverse (trace and retrace) over the same region of a SWNT, it is also possible to assess any blocking of EC activity by serotonin oxidation reaction products. At a physiologically relevant concentration (5 μM), there is no detectable blocking of SWNTs, which can be attributed, at least in part, to the high diffusion rate to an individual, isolated SWNT in the SECCM format. At higher serotonin concentration (2 mM), oligomer formation from oxidation products is much more significant and major blocking of the EC process is observed from line profiles recorded as the SECCM meniscus moves over an SWNT. The SECCM line profile morphology is shown to be highly diagnostic of whether blocking occurs during EC processes. The studies herein add to a growing body of evidence that various EC processes at SWNTs, from simple outer sphere redox reactions to complex multi-step processes, occur readily at pristine SWNTs. The platform described is of general applicability to various types of nanostructures and nanowires.

Introduction

The use of carbon nanotubes (CNTs) as electroactive materials in sensors and biosensors is of increasing interest, especially as a consequence of their chemical stability, high electrical conductivity, low price, biocompatibility and wide potential window.1 Yet, the rational integration of CNTs into electrochemical sensors has been limited, until recently, by a lack of appropriate experimental tools with which to develop and assess fundamental models for electrochemistry at CNTs. The

majority of experimental studies, focused on macroscopic measurements of large ensembles of CNTs,[1, 2] have claimed that, even for simple outer sphere redox couples, heterogeneous electron transfer (HET) only takes place at edge-plane defects in multi-walled nanotubes,[3] or at opened oxygenated ends of single walled nanotubes (SWNTs).[4, 5] The sidewall – which constitutes the main area of an SWNT - has been proposed to be inert towards HET.[2-5] On the other hand, microscopic measurements at individual SWNTs have suggested highly active sidewalls for electrochemistry,[6-9] in agreement with the response observed at other types of sp^2 carbon electrodes such as the basal surface of highly oriented pyrolytic graphite (HOPG)[10-18] or graphene,[19] which also exhibit high activity to HET.

Measurements at individual SWNTs are evidently much less ambiguous than those on macroscopic samples which typically average over millions of different CNTs. The first attempts to isolate and study the electrochemistry of an individual SWNT involved defining an electrochemical cell over a single nanotube by lithographic means.[6] Recently, we proposed an alternative approach, using scanning electrochemical cell microscopy (SECCM),[20, 21] a pipette-based technique developed in our group, to confine the electrochemical (EC) measurement to small regions of an SWNT.[8, 9] The convenience of this approach for the study of individual SWNTs resides in the EC cell being defined by a liquid meniscus at the tapered end of a double-barrelled pipette used as a probe, the size of which is easily tuneable from microns to tens of nanometres. Not only does this confer high spatial resolution, but also minimizes the need to manipulate or prepare the sample, hence allowing it to be studied in close to its pristine state. In addition, the scanning capability of the moveable EC cell allows maps of EC activity to be built up, facilitating the determination of structure-activity correlations.[10, 19, 22] Thus, SECCM has been used to study HET on 2-D networks of pristine SWNTs grown by catalysed chemical vapour deposition (cCVD) on inert Si/SiO_2 supports.[8] By tuning the dimensions of the SECCM probe, it was possible to access SWNT sidewalls, ends and cross junctions and assess the electrochemistry of two different outer sphere redox mediators[8] without any influence from (or need of) a support electrode.

Very recently, we have developed a new platform, combining flow-aligned SWNTs on Si/SiO_2 substrates with SECCM,[9] allowing the EC response to be mapped, together with a complete characterisation of the SWNT,[6, 9] including the electronic properties, which can be either semiconducting or conducting.[23, 24] This is a key aspect which tends to be ignored in macroscopic measurements of SWNT ensembles.

The aim of this paper is to build significantly on this new approach by considering more complex EC processes, such as multistep processes involving HET and coupled chemical steps, as in the detection of neurotransmitters which is the focus herein. CNTs have generally been demonstrated as a suitable carbon-based electrode material for the detection of neurotransmitters, such as serotonin[25] (which plays a key role in numerous physiological processes, such as depression[26]) and dopamine.[27, 28] Very low limits of detection are possible when SWNT network ensembles are used,[27] however the extent to which such complex processes are controlled by particular features on SWNTs is not well understood. Moreover, particularly in biosensing applications, carbon electrodes may suffer from fouling from reaction, intermediates or products,[25, 29, 30] which is a key problem to assess when considering the future applications of SWNTs as *in-vivo* or *in-vitro* sensors or in long-term implants.

In this paper, we have used the individual SWNT platform, combined with SECCM,[20, 21] to investigate the oxidation of serotonin. The high mass transport achievable with this platform[8, 9, 31] has allowed us to study this complex multi-step reaction[32, 33] and determine the activity of SWNT sidewalls and the impact of fouling by side reactions. The platform described allows an individual SWNT electrode to be selected, and fully characterised with complementary techniques such as Raman spectroscopy, AFM and conductance measurements, paving the way to understand how surface structure and the electronic nature of an SWNT impact EC activity.

Experimental

Sample preparation: Flow aligned SWNTs were grown on Si/SiO_2 (IDB Technologies Ltd.; n-type Si, 525 μm thick with 300 nm of thermally grown SiO_2) by cCVD, using Fe catalyst nanoparticles.[8] Each substrate was partially immersed in an aqueous solution of horse spleen ferritin protein (Sigma Aldrich) diluted 1:200 from the original concentration for 20 minutes, resulting in a band of catalyst nanoparticles along one side of the substrate (Figure 1A). The substrates were air dried in a nitrogen stream and ashed in an oxygen plasma for 2 minutes at 100 W (K1050X plasma system, Emitech, UK) before being placed into a cold wall cCVD system (Moorfields, UK), in which the samples were positioned directly onto the heating element, while the surrounding wall remained at a much lower temperature (<100°C). The samples were oriented with the band of catalyst nanoparticles perpendicular to the direction of flow since nanotubes grow along the direction of gas flow,[34, 35] Figure 1B. Samples were heated to 950°C under a flow of 150 sccm H_2 and 250 sccm Ar for 5 minutes. The growth period was initiated upon the introduction of ethanol to the system via a flow of 250 sccm Ar, bubbled through ethanol at 0°C, whilst maintaining the flow of H_2 at 150 sccm. The duration of this growth phase was set between 5 and 10 minutes, depending on the desired nanotube length. After this period, the flow of Ar-ethanol and H_2 was terminated and the system was left to cool under a flow of 1000 sccm of Ar.

Metal contacts: The macroscopic electrical contact to the SWNTs was provided by a thermally evaporated (Minibox, Moorfields, UK) Pd band (~70 nm thick) with an adhesion layer of 2 nm of Cr. The area to be covered was defined by a stencil shadow mask, ensuring that the SWNTs remained pristine in the region of interest (ROI).

Silver electrodepostion: To confine the electrodeposition, a single barrel pipette was used to define the electrochemical cell, as described in Figure 2A.[34] Briefly, a single channel glass pipette of approximately 200 μm tip opening was produced by laser-pulling (P-2000 Sutter Instruments) followed by polishing.[34] The pipette was filled with an aqueous solution (made up in Millipore Milli-Q water for all solution in this study) of silver nitrate (10 mM) and supporting electrolyte (50 mM KNO_3), together with a silver wire electrode that acted as a quasi-reference counter-electrode (QRCE). The pipette was then approached to the sample by means of a micropositioner *x-y-z* stage (Newport, USA) until the formation of a meniscus between the pipette and sample, defining an electrochemical cell. This was then moved laterally across the substrate, parallel to the thin metal contact, while a potential of -0.3 V was applied to the sample with respect to the QRCE in the pipette. Under these conditions, a change in the current was observed when a section

of a SWNT (serving as a working electrode) was wetted by the meniscus, with the reduction of silver ions to silver particles taking place at the surface of the SWNT. Figure 2B shows a field-emission scanning electron microscopy (FE-SEM) (Zeiss Supra-55) image of an aligned SWNT decorated by silver particles.

Atomic Force Microscopy (AFM): Tapping-mode AFM imaging (Enviroscope, Bruker-Veeco, USA) was performed over pristine regions of the SWNTs under investigation (Figure 2C, bottom).

Hg-ultramicroelectrode (Hg-UME) probe fabrication: A liquid mercury hemisphere was electrodeposited at the tip of a disc-shaped glass-sealed and polished platinum ultramicroelectrode (UME), of 12.5 μm radius. In Figure 3A a schematic and an optical image of an Hg-UME probe (Hg hemisphere of 12.5 μm radius) is presented. The electrodeposition was carried out by means of a potentiostat (CH Instruments, 730A, TX, USA) in a two-electrode EC cell using the UME as a working electrode and silver wire as QRCE in an aqueous solution of 10 mM mercurous nitrate (Acros organics) in 50 mM nitric acid (Fisher Scientific).[36] The Hg-UME probe was mounted on a manual *x-y-z* micropositioner that was used to approach and scan the probe across the sample. The silver particles facilitated the rough localisation of the SWNT and minimised the area of the sample that had to be scanned to seek the SWNT of interest. A potential bias of -0.5 V was applied between the Hg-UME probe and ground, while the sample (SWNT) at ground (Figure 3A). This ensured that an electronic current would flow through both metallic and semiconductor SWNTs (*vide infra*). Once an electrical contact between the protruding Hg drop and the SWNT was made, evidenced by a current flow, the probe position was fixed and current-voltage curves were measured (CH Instruments, 730A, TX, USA). At this point, the relative potential difference between the Hg-UME and the substrate was scanned (at 100 mV s^{-1}) between +3 and -3 V, producing current-voltage curves that were used to determine the electronic nature of the SWNT.

Multiple contact SWNT device: For very low densities (one SWNT per cm^2 of sample), multiple metal contacts were applied over the SWNT employing a shadow mask with two (or more) windows to delimit the area of the thermal deposition of metal film (Pd). The visualisation of the silver electrodeposit aided the alignment of the mask (perpendicular to the SWNT) and ensured that there was only one SWNT bridging the metals contacts. An example of a typical device with multiple contacts (separated by different distances) is presented in Figure 3B.

Microcapillary electrochemical method measurements: A single barrel pipette was laser-pulled (P-2000, Sutter Instruments) to a sharp end and polished flat until a tip opening of 50 μm in diameter was obtained.[34] Two one-electron outer sphere redox couples were employed: the oxidation of ferrocenylmethyl-(trimethylammonium) ($FcTMA^+$), as the hexafluorophosphate salt synthesised in-house[37] and the reduction of ruthenium(III) hexamine ($Ru(NH_3)_6^{3+}$) (as the chloride, Strem Chemicals, Newbury Port, USA). The pipette was filled with 2 mM $FcTMA^+$ salt and 2 mM $Ru(NH_3)_6^{3+}$ salt and supporting electrolyte (100 mM KCl), together with a chloridized Ag wire as a QRCE. In a similar manner as for the silver decoration of SWNTs (see above), the probe was scanned across the sample, perpendicular to pristine sections of the SWNTs, in a region between the Pd contact and Ag decoration, while a potential for $FcTMA^+$ oxidation of 0.3 V vs. Ag/AgCl QRCE was applied via a potentiostat (CH Instruments, 730A, TX, USA), giving an EC current for both metallic and semiconducting SWNTs when in contact with the solution.[34] Once the moveable EC cell was centred over the SWNT of interest, a

wide potential range cyclic voltammogram (CV) was measured to determine the activity (or not) towards $Ru(NH_3)_6^{3+}$ reduction, which was used to determine the electronic nature of the nanotube (*vide infra*).

Scanning Electrochemical Cell Microscopy: A complete description of SECCM can be found elsewhere.[9, 10, 15, 19-21, 31] SECCM employed double-barrel borosilicate glass pipettes as probes. These were pulled to a sharp taper by means of a laser puller (see above), yielding an opening of a desired size. In the present study, probes between 400 to 1000 nm were used, the dimensions of which were precisely determined by FE-SEM. To ensure a confined and stable meniscus contact during experiments, the outer walls of the pipette were silanised using dimethyltrichlorosilane (Aldrich). Then, both barrels of the pipette were filled with solution (5 μM - 2 mM serotonin hydrochloride (Sigma-Aldrich) in 10 mM HEPES buffer and 0.1 M NaCl), and a chloridized silver wire was inserted into each barrel, which acted as a QRCE. A potential bias (V_2 in Figure 3C) was applied between the QRCEs (0.5 V in the present study) to induce an ion conductance current across the thin film layer of solution protruding from the tapered end of the probe that connected both barrels. The probe was then mounted on a highly controllable *x*,*y*,*z* piezoelectric positioning instrument (for *z*-axis P-753.31C, *xy*-axis P-622.1CD, Physik Instrumente), with the sample positioned vertically below the probe. The probe was oscillated (typical frequency 266 Hz, peak to peak oscillation approximately 50 nm) in the *z*-direction (perpendicular to the sample surface) to generate an alternating component (AC) of the ion conductance current (I_{IC}) upon meniscus contact with the surface. As described in detail elsewhere,[20, 31, 38] this is due to the periodic motion of the meniscus changing the dimensions of the conductance cell. The AC component (magnitude) was extracted with a lock-in amplifier (SR830, Stanford Research Systems) and used to maintain a constant tip-sample separation during imaging due to the strong dependence of the AC amplitude on the tip-sample separation with meniscus contact.[20, 31]

With the meniscus at the end of the pipette in contact with the substrate, the moveable EC cell was translated laterally across the surface at a speed of 0.5 μm s^{-1}, while measuring the surface EC current (I_{EC}).[21] A schematic of the whole SECCM setup is presented in Figure 3C.

To drive electrochemical reactions at the SWNT, a bias V_1 (see Figure 3C) was applied so that the effective potential applied to the SWNT was $-(V_1+V_2/2)$ with respect to the QRCE. The sample was mounted so that the main scan axis (*x*-axis) was essentially perpendicular to the SWNT of interest. The scan pattern was designed so that the meniscus moved forward and reverse over the same line before moving to a new line, allowing for the identification and validation of EC features, but also enabling any changes in surface activity to be identified.

Raman spectroscopy: A 514 nm laser micro-Raman spectroscopy set up (Argon laser, 10 mW, 50x lens, NA 0.85, inVia micro-Raman, Renishaw, UK) was employed for the acquisition of Raman spectra over pristine sections of the SWNTs, roughly localized by the silver deposit.

RESULTS AND DISCUSSION

SWNT synthesis and characterisation

A key feature of the platform employed herein is that SWNTs were investigated in their pristine state and fully characterised. To achieve this, it was essential that steps

such as the establishment of electrical contacts with the SWNTs and marking of parts of SWNTs via silver particle decoration to enable rough localisation (*vide infra*), were done with minimal manipulation or perturbation of the SWNTs. Millimeter-long straight SWNTs were ideal for this purpose: their long lengths enabled the use of metal thin film contacts, deposited with stencil shadow masks, avoiding photolithography or other techniques that could leave residues on the parts of the SWNT to be investigated electrochemically. In addition, the employment of long SWNTs allowed the establishment of a large pristine ROI set far from the catalyst (contact) region, ensuring that the electrochemical response was free from any contribution of the catalyst particles from which the SWNTs were grown.

Various methods based on cCVD have been developed for growing horizontally aligned ultra-long SWNTs in the last few years.[35] Gas-flow-guided growth[39-41] or the use of a quartz single crystal substrate for lattice-induced growth[42, 43] are some of the strategies used to achieve aligned arrays of SWNTs of large length. For the studies herein, flow alignment was used, as this provided flexibility in the substrate to be used and offered the production of SWNT arrays of lower density, facilitating access to individual SWNTs by SECCM and other techniques.

To obtain flow-directed horizontally-aligned ultra-long SWNTs, physical aspects of the process to maintain the SWNT floating, or lifted, above the substrate during growth needed to be considered, such as fast-heating[41, 44, 45]or ultralow feeding gas.[34, 46] We used a cold-wall cCVD system[9] (Figure 1B), in which only the heating plate where the sample was positioned - located at the centre of the chamber - reached the growth temperature. This system allowed fast-heating[41, 44, 45] (from room temperature to 950˚C in 7 min), generating local turbulences that are believed to facilitate the "take off" of the nanotube-catalyst and maintain it lifted above the substrate during growth.[41, 44, 45] As a catalyst, Fe nanoparticles derived from ferritin solution were used,[8, 9] rather than very active and commonly used Cu,[47] so as to achieve a low density of SWNTs on the sample,[40, 47] thereby minimising SWNT overlap and the formation of bundles during flow growth.

Using the growth conditions described in detail in the experimental section, straight flow-aligned millimetre long SWNTs were grown on Si/SiO_2 surfaces. Interestingly, the growth direction was towards the gas flow, in contrast with the common conception in the literature that it is with the flow.[35, 40, 48, 49] This suggests a tip-growth mechanism,[40] where the catalytic particle is at the flying end of the SWNT. Once the particle-nanotube reached a certain height, where there is a stable laminar gas flow regime,[50] the SWNT grows fairly straight for long distances, and its growth terminates when the flying SWNT falls to the substrate, possibly bouncing and rolling, in a turbulent regime, introducing to the end of the SWNT a tortuous twisting (Figure 1C). Different growth times were evaluated, and it was concluded that maximum growth occurred within the first 5-10 min; extending the growth for longer periods neither increased the SWNT density nor the length of SWNTs.

Visualisation of SWNTs by local silver electrodeposition

To enable ready visualisation of the SWNTs by optical microscopy, silver particles were electrodeposited on a section of the SWNTs (see Experimental section), creating an ensemble of particles that marked one end of the SWNT (away from the Pd contact). Ensembles of particles were visible under FE-SEM (Figure 2B) and optical microscopy (Figure 2C, top), allowing the rough localization of the SWNT and, in particular, an indication of the location of the pristine segment of the SWNT.

Tapping-mode AFM of the nanotubes (Figure 2C) was carried out confirming the cleanliness of the sample and the area of interrogation (lack of residues and catalytic particles), and to determine the diameter of the nanotube. In the study herein, SWNTs were around ~1.2 nm in diameter, in agreement with the single-walled nature and the type of cCVD growth.[8, 9]

Electronic characteristics of individual SWNTs

We consider and assess three different methods to identify the electronic character of individual SWNTs. First, conductance measurements were made by recording current (I) – voltage (V) curves across a defined portion of an SWNT. For metallic SWNTs, which could approach quantized conductance values at room temperature, there is often significant additional resistance at the metal contacts[51] or due to SWNT defects, giving rise to ohmic response with variable resistance values.[52] In contrast, for semiconductor SWNTs, that are considered p-type semiconductors,[53] the overlap of the metal-SWNT electronic states results in the presence of a Schottky barrier at the metal contact-semiconductor interface for hole or electron injection.[52] The value of this barrier depends on the band alignment at the metal-SWNT interface, and assuming the absence of interface states,[54] is determined by the work function of the metal contact, the work function of the SWNT (aprox 4.9 eV) and the band gap of the SWNT.[54] Thus, a metal with large work function such as Pd (5.1 eV), which we selected specifically for the studies herein, tends to form an ohmic contact for hole injection[55] because the Fermi level of the metal lies within the valence band of the SWNT. For the SWNTs used in this work this is particularly applicable because they are of relatively large diameter, which results in a small band gap.[24] It is worth noting that high work functions alone might not be sufficient to ensure an ohmic contact, as observed for Pt, which due to poor wetting with the SWNT introduces additional tunnelling barriers.[56] Under these conditions, the response to hole injection is ohmic, whilst a large barrier exists to electron injection, leading to an asymmetry in the conductance I-V curves, with the device behaving as a rectifier or Schottky diode.[52, 57] This is evident in the resulting I-V curves that were used to assess the electronic nature of SWNTs.[58] In Figure 5A, two representative I-V curves for a metallic (top) and semiconductor (bottom) SWNTs are presented, the former exhibiting a defined ohmic response, while the latter displays a rectifying behaviour, with small leakage current.[9]

An alternative technique to elucidate the electronic nature of CNTs is Raman spectroscopy.[59] Besides the ability to distinguish between metallic and semiconducting SWNTs,[60] a vast amount of information about CNTs can be obtained,[59] but for our purposes, we focused on two of the most important signals in the Raman spectra of SWNTs: the radial breathing mode (RBM) region, between 100 and 300 cm^{-1}, corresponding to the coherent vibration in the radial direction; and the G-band region found around 1580 cm^{-1}. The presence of peaks in the RBM region confirmed the single-walled nature of the CNTs under investigation, and the peak frequency was used to estimate the SWNT diameter,[61] resulting values in agreement with the ones obtained with AFM (~1.2 nm).

Figure 4 shows how metallic and semiconducting SWNTs can be distinguished by focusing on the G-band region. Usually composed by two peaks, G+ (feature associated with carbon atom vibrations along the SWNT axis) and G− (feature associated with vibrations of carbon atoms in the circumferential direction), the metallic SWNTs G-band is composed by two components, one peak at 1590 cm^{-1}

(denoted G+) and another broader and asymmetric peak with the Breit-Wigner-Fano lineshape, at lower frequency (labelled G-).[62] Semiconducting SWNTs, however, exhibit two intense Lorentzian lineshapes in the G-band region.[60] In addition, the high quality and essentially defect-free nature of the SWNTs synthesized herein was confirmed by the lack of any peak in the D-band around ~1350 cm^{-1}.

Recently, we have reported the use of SECCM[8, 9, 63] to determine the EC activity of SWNTs for two well-known and widely studied outer-sphere redox processes, the one-electron oxidation of $FcTMA^+$ and the one-electron reduction of $Ru(NH_3)_6^{3+}$, demonstrating the high electrochemical activity of pristine SWNT sidewalls. While both metallic and semiconductor SWNTs exhibited very high kinetic rate constants towards the oxidation of $FcTMA^+$, a huge difference between the EC current at metallic and semiconducting SWNTs was observed for the reduction of $Ru(NH_3)_6^{3+}$. The EC current was consistent with high activity at metallic SWNTs, but for semiconductor SWNTs the current was almost undetectable (except at high driving potentials where a small current was seen),[9] due to the redox potential of the $Ru(NH_3)_6^{3+/2+}$ couple lying in the charge depletion region of semiconducting SWNTs.[36] The simultaneous employment of these two redox couples in solution can thus be used to distinguish easily between metallic and semiconductor SWNTs.

Figure 5B and 5C shows two typical CVs obtained with a 50 μm diameter single barrel pipette filled with both redox couples (2 mM each of $FcTMA^+$ and $Ru(NH_3)_6^{3+}$), one carried out on a metallic SWNT (B) and the other on a semiconducting SWNT (C). Both responses show a clear sigmoidal signature for the $FcTMA^{+/2+}$ couple, but exhibit a strong difference in the cathodic region, with a voltammetric signature for $Ru(NH_3)_6^{3+}$ reduction only seen for the metallic SWNT. This confirms the suitability of this experiment to distinguish between metallic and semiconducting SWNTs.

Oxidation of serotonin

We used the platform outlined to study the EC response for serotonin EC oxidation at individual metallic SWNT. We selected metallic SWNTs because these are most useful for general electrochemical analysis, as highlighted above.

A typical SECCM image for the oxidation of 5 μM serotonin (in 10 mM HEPES and 0.1 M NaCl) is presented in Figure 6A. The map of EC activity, acquired at an effective potential of 0.55 V vs. Ag/AgCl QRCE (just below the diffusion-limited potential, corresponding to ca. 80-90% of the limiting current value), shows a clear and uniform response along the entire length of the SWNT. Considering the type of SWNT employed in this work and the lack of D-peak in the Raman spectrum (Figure 4), the measured current cannot be attributed uniquely to EC oxidation at defect sites, which are found at a very low density (one defect per 4 μm on average).[64] Thus, the SWNT sidewalls promote the EC oxidation process, as seen for other neurotransmitters on sp^2 carbon electrodes generally.[12-14, 16, 25] Indeed, the studies herein, together with other reports,[6-9] indicate clearly that the sidewalls of SWNTs can easily support various redox reactions spanning simple outer-sphere couples and more complex multi-step processes.

The orientation of the moveable SECCM probe with respect to the SWNT during imaging means that scan profiles can be analysed to extract further spatially resolved EC information, since the redox current is collected at 1 nm intervals along each line scanned by the pipette meniscus. Comparing the trace and retrace EC maps and considering the corresponding line profiles (Figure 6A), highly consistent behaviour

is observed. As the meniscus moves from the inert substrate (Si/SiO_2) to the active SWNT, the EC current gradually increases as the length of the nanotube accessed by the SECCM meniscus increases, with the current reaching a peak value when the SWNT lies at the centre of the meniscus from the pipette. The consistency of the trace and retrace scan images and the morphology of the line profiles (as expected for an active surface without any parasitic blocking process[9]) indicates that on this timescale (ca. 1.8 s total contact time of the meniscus with the SWNT in each pass for this particularly experiment) and serotonin concentration (5 μM) the SWNT remains highly active for electrochemistry.

It is important to point out that although the concentration of serotonin is low, the electrode is submitted to very high mass transport[8, 9, 31] yielding high peak current densities (~5.5 mA cm^{-2} considering that the entire area of the SWNTs was fully accessible), yet there is minimial (undetectable) fouling on the timescale of the experiment. The absence of fouling effects may be attributed to the extremely high mass transport to and from the SWNT electrode surface,[8, 9, 31] which facilitates the diffusion of the fouling products away from the electrode in this configuration before blocking can occur.[9] The serotonin oxidation process (Figure 6B) also involves a side reaction (not shown) leading to oligomer formation (Figure 6C).[33] The high mass transport rates of the SECCM/SWNT configuration means that this side reaction can be outrun at low serotonin concentration. In fact, these results highlight the considerable potential of individual SWNTs as an electrode material of high activity that is relatively immune to fouling in the detection of neurotransmitters. Fouling by reaction products can be minimised by simply enhancing mass transport of the species generated rather than needing to use preconditioning potentials or alternative materials (or surface functionalities). It is interesting to note that the configuration of a moving meniscus and individual SWNT also opens up the detection of trace amounts of material. The profiles in Figure 6A correspond to the detection of just ~320 fC of charge. For the ($2e^-$) oxidation of serotonin (Figure 6B) this equates to attomol detection levels, and even lower quantities are open to measurement based on the excellent signal to noise observed.

In order to investigate the impact of film formation on the resulting EC properties of SWNTs, deliberately higher concentration of serotonin (2 mM) were employed in order to accelerate blocking film formation. In Figure 7A, EC activity maps (trace and retrace) of serotonin EC oxidation at an individual metallic SWNT are shown, acquired at the same potential as for Figure 6A (effective potential 0.55 V vs. Ag/AgCl QRCE in 10 mM HEPES buffer and 0.1 M NaCl). EC activity is again seen along the entire length of the SWNT, but due to the higher concentration, we observe different maps and line profiles from those seen in Figure 6A. These are consistent with rapid fouling of the SWNT as soon as meniscus contact is made. Based on the data in Figure 6A, one would predict a peak current of 80 pA, but – in fact – after increasing rapidly upon meniscus contact with the SWNT (left hand edge of the image and profile in Figure 7A), the current decreases rapidly with further meniscus contact, and with the meniscus directly centred over the SWNT, the current is less than 10% of the value expected. Thus, once the meniscus makes contact with the SWNT and serotonin oxidation begins, the current decays due to fouling of the surface, despite the increasing area of the SWNT exposed to solution during imaging. This leads to a large asymmetry in the SECCM line profile shape.

The impact of the fouling products on the EC process at the SWNT is further

confirmed with the retrace scan profiles, which do not exhibit the initial current spike (seen on the trace scan when the meniscus made initial contact) since the SWNT is already extensively fouled (Figure 7B). The initial current in the retrace scan corresponds closely to that measured at the end of the trace linescan.

Taken together, the data in Figure 6A and 7A highlight how SECCM can be used to assess complex EC processes. Moreover the platform opens up a new route to trace EC detection of neurotransmitters at physiologically relevant concentrations, without any blocking effects which impact other EC techniques and carbon electrodes. Indeed, voltammetric measurements at conventional carbon electrodes struggle to achieve detection at the μM level by voltammetric methods,[29] yet an individual SWNT opens up this possibility (Figure 6A). If, over large time periods, the SWNTs were to become contaminated, the pipette could simply be moved to another part of the SWNT or to another SWNT, suggesting SWNT arrays coupled with droplet cells as a new approach to trace electroanalysis.

CONCLUSIONS

SECCM imaging of individual metallic single-walled carbon nanotubes (SWNTs) has revealed that the sidewalls are highly electrochemically active for the oxidation of serotonin, a complex, multi-stage process involving coupled heterogeneous electron transfer and chemical steps. No signs of electrode fouling were observed when physiologically relevant concentrations of serotonin were used (5 μM), although there was a deleterious impact of the EC process at much higher concentrations (2 mM) where the formation of blocking oligomers became more significant. This was readily seen in the morphology of the EC images recorded which indicated rapid fouling as soon as the SECCM meniscus made contact with the SWNT.

An important feature of the platform described is that a particular type of SWNT can be selected and investigated. We have presented 3 different ways in which a metallic and semiconducting SWNTs can be identified and distinguished. First, the platform described enables micro-Raman spectroscopy to be applied to individual SWNTs, with the spectra recorded allowing the SWNT diameter and basic electronic characteristic to be determined. Second, we have shown how a mobile Hg-contact can be used as one terminal in a 2-terminal device in which electronic conductance *I-V* curves can be measured, from which an SWNT can be assigned as semiconducting or conducting. Third, the outer-sphere redox couple $Ru(NH_3)_6^{3+/2+}$ is very sensitive to the electronic character of an SWNT. In all cases, the SWNT can be located by these techniques and, by SECCM, because one end of an SWNT can be marked by Ag electrodeposition for detection by optical microscopy.

The field of electrochemistry at SWNTs has been held back for some time by the difficulty of studying individual well-characterised SWNTs, a general inability to link electrochemistry to the electronic properties of the SWNT, and a lack of suitable high resolution EC methodologies to probe electrochemistry at a length scale that is capable of resolving any role of defects, or other features of SWNTs, in the EC behaviour. The platform described allows these issues to be addressed and overcome, thereby greatly advancing understanding of the electrochemistry of SWNTs. Moreover, the platform should be applicable to other types of nanostructures which are of growing interest for EC technologies and fundamental charge-transfer studies.

ACKNOWLEDGMENTS

This project was supported by the European Research Council through Project ERC-2009-AdG 247143-QUANTIF and EPSRC (EP/H023909/1 and MOAC CDT studentship), with additional support from the National Physical Laboratory. JCB acknowledges a Marie Curie International Incoming Fellowship under project number 329953 "POLYMAP". Equipment used in this research was obtained through Science City (AM2), with support from Advantage West Midlands and partial funding by the European Regional Development Fund.

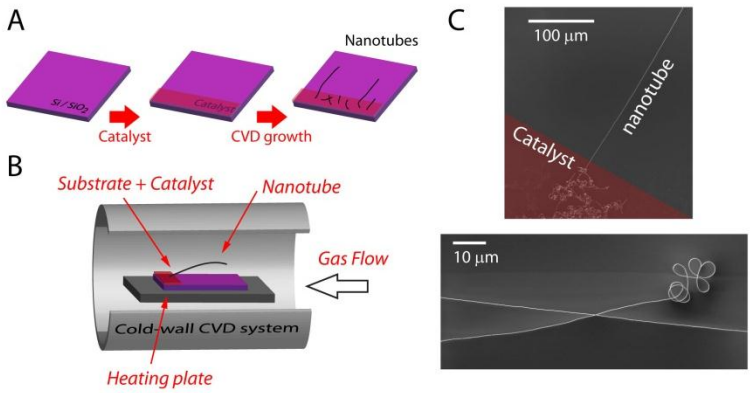

Fig. 1 (A) Si/SiO_2 wafers were used as substrates for carbon nanotube growth. The catalyst (ferritin) was deposited to only one edge of the sample, from where SWNTs were grown by cCVD over the region that is catalyst free. (B) Schematic of a cold-wall cCVD system, where a heating element heats the sample. The sample was placed so that the area with catalyst was away from the flow since the SWNTs grew against the flow. (C) FE-SEM images of flow aligned SWNTs. Straight long nanotubes (top) were synthesized, that were terminated in a tortuous shape (bottom).

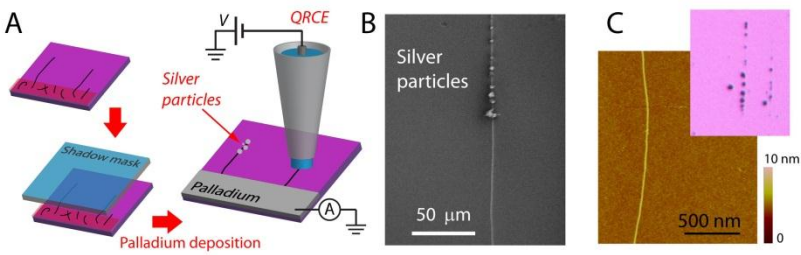

Fig. 2 (A) A shadow mask was used to select an area to be covered with a Pd thin film co-incident with catalyst region. Once electrical contact had been made to the SWNTs, silver decoration of SWNTs was carried out by means of a single barrel pipette filled with $AgNO_3$ and KNO_3 and a silver wire acting as QRCE. A pristine length of SWNT between the macroscopic metal thin film and the silver nanoparticles was interrogated by complementary techniques. (B) FE-SEM image of a SWNT showing a silver decorated section and a pristine segment. (C) The silver particles can be easily visualised by optical microscopy (top) and the pristine area of the nanotube interrogated by AFM (bottom) is clean and free from residues and catalyst.

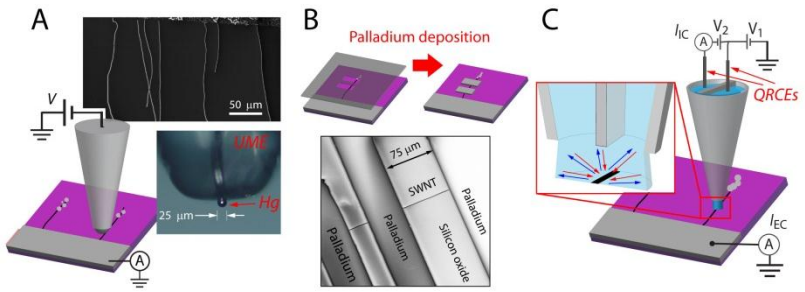

Fig. 3 (A) FE-SEM image of an array of flow-aligned SWNTs. The density required the use of a Hg-UME probe to electrically contact each SWNT individually. Schematic of the experimental setup, with a UME with a Hg drop (optical image). (B) Stencil shadow masks were employed in devices with one SWNT per sample. The silver particles facilitated the localization of the SWNT and the correct placement of the shadow mask. FE-SEM image of a device with three Pd contacts along one single SWNT. (C) Schematic of the SECCM operation: double barrel pipette filled with the solution of interest and one chloridized silver wire in each barrel acting as QRCEs. SECCM was deployed in the pristine region of the SWNT. The combination of SECCM and SWNT provides high mass transport towards and away from the SWNT.

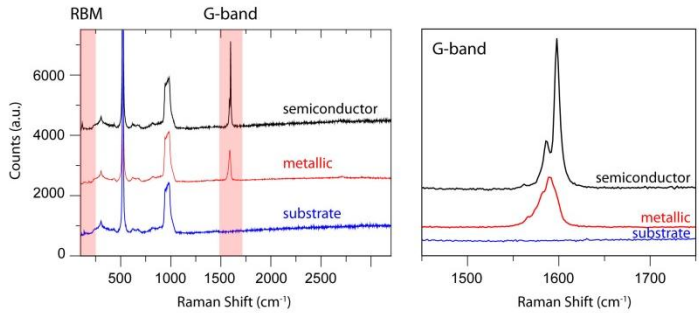

Fig. 4 Comparison of Raman spectra acquired on metallic (red line) and semiconducting (black line) SWNTs, as well as the supporting substrate (Si/SiO_2, blue line). The RBM and G-band regions are indicated with a light red box. The major difference in the Raman spectra between metallic and semiconducting SWNTs is found in the G-band region, both in shape and intensity, as shown in right-hand-side plot.

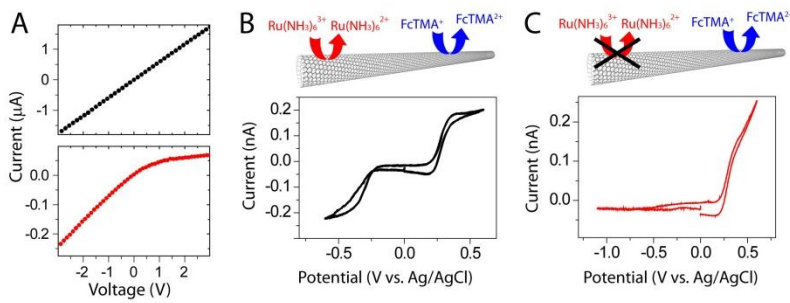

Fig. 5 (A) Representative current-voltage traces for a metallic (top) and semiconductor (bottom) SWNT. Voltage applied to the mobile mercury contact with respect to the sample. Interrogation of the EC activity on pristine individual SWNTs using a single barrel pipette (~50 μm diameter) filled

with two mediators, 2 mM $FcTMA^+$ and 2 mM $Ru(NH_3)_6^{3+}$, and supporting electrolyte (0.1 M KCl), and a Ag/AgCl wire as a QRCE. Cyclic voltammograms (100 mVs^{-1}) on a metallic (B) and semiconductor (C) SWNT.

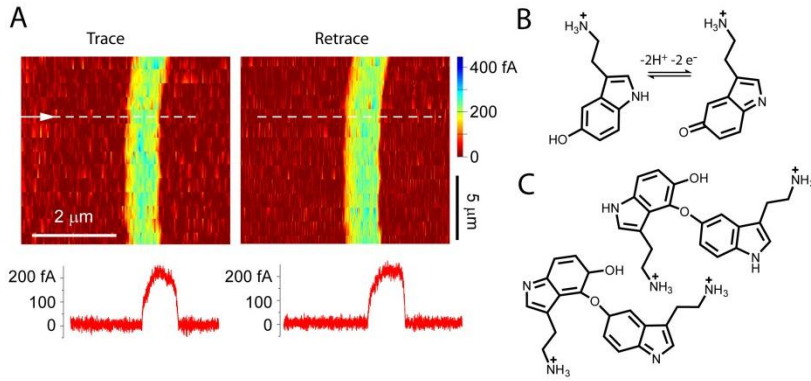

Fig. 6 (A) SECCM maps of EC current (trace –left and retrace –right) of the oxidation of serotoinin (5 μM in 10 mM HEPES buffer and 0.1 M NaCl) acquired at 0.55 V vs. Ag/AgCl QRCE at a pipette scan velocity of 0.5 μm s^{-1}. Corresponding scan profiles (line plotted marked with an arrow) are also shown. (B) Scheme for the two-electron two-proton oxidation of serotonin. (C) Two examples of the major dimers formed in side reactions suggested to lead to insoluble polymer-like by-products.[33]

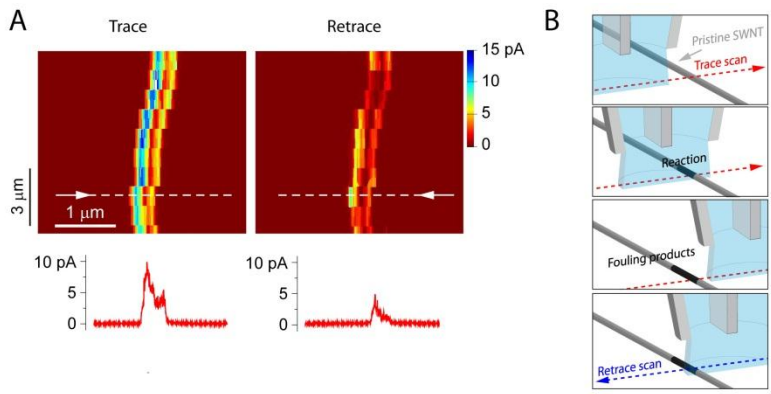

Fig. 7 (A) SECCM maps of EC current (trace –left and retrace –right) of the oxidation of serotonin (2 mM in 10 mM HEPES buffer and 0.1 M NaCl) at 0.55 V vs. Ag/AgCl QRCE on an individual SWNT. The asymmetry in the scan profiles is proof of the fouling of the electrode. Scan profiles plotted are marked with an arrow. (B) Sequence of processes during a line profile measurements: the fouling products generated in the trace scan remain on the SWNT and on the retrace the SECCM meniscus scans over a fouled electrode.

References

[a] *Department of Chemistry, University of Warwick, Gibbet Hill Road, Coventry, CV4 7AL, United Kingdom. Tel:+44 (0) 2476 523264; E-mail: p.r.unwin@warwick.ac.uk*
[b] *Molecular Organisation and Assembly in Cells Doctoral Training Centre, University of Warwick, Gibbet Hill Road, Coventry, CV4 7AL, United Kingdom.*

1. I. Dumitrescu, P. R. Unwin and J. V. Macpherson, *Chem. Commun.*, 2009, **45**, 6886-6901.
2. R. L. McCreery, *Chem. Rev.*, 2008, **108**, 2646-2687.
3. C. E. Banks, T. J. Davies, G. G. Wildgoose and R. G. Compton, *Chem. Commun.*, 2005, 829-841.
4. A. Chou, T. Bocking, N. K. Singh and J. J. Gooding, *Chem. Commun.*, 2005.
5. C. E. Banks, R. R. Moore, T. J. Davies and R. G. Compton, *Chem. Commun.*, 2004, 1804-1805.
6. I. Heller, J. Kong, H. A. Heering, K. A. Williams, S. G. Lemay and C. Dekker, *Nano Letters*, 2005, **5**, 137-142.
7. J. Kim, H. Xiong, M. Hofmann, J. Kong and S. Amemiya, *Anal. Chem.*, 2010, **82**, 1605-1607.
8. A. G. Güell, N. Ebejer, M. E. Snowden, K. McKelvey, J. V. Macpherson and P. R. Unwin, *Proc. Natl. Acad. Sci. USA*, 2012, **109**, 11487-11492.
9. A. G. Güell, K. E. Meadows, P. V. Dudin, N. Ebejer, J. V. Macpherson and P. R. Unwin, *Nano Lett.*, 2014, **14**, 220-224.
10. S. C. S. Lai, A. N. Patel, K. McKelvey and P. R. Unwin, *Angewandte Chemie, Intl. Ed.*, 2012, **51**, 5405-5408.
11. A. N. Patel, M. G. Collignon, M. A. O'Connell, W. O. Y. Hung, K. McKelvey, J. V. Macpherson and P. R. Unwin, *J. Am. Chem. Soc.*, 2012, **134**, 20117-20130.
12. A. N. Patel, K. McKelvey and P. R. Unwin, *J. Am. Chem. Soc.*, 2012, **134**, 20246-20249.
13. A. N. Patel, S.-y. Tan, T. S. Miller, J. V. Macpherson and P. R. Unwin, *Anal. Chem.*, 2013, **85**, 11755-11764.
14. A. N. Patel, S.-y. Tan and P. R. Unwin, *Chem. Commun.*, 2013, **49**, 8776-8778.
15. P. M. Kirkman, A. G. Güell, A. S. Cuharuc and P. R. Unwin, *J. Am. Chem. Soc.*, 2014, **136**, 36-39.
16. S. Lhenry, Y. R. Leroux and P. Hapiot, *Anal. Chem.*, 2012, **84**, 7518-7524.
17. A. Anne, M. A. Bahri, A. Chovin, C. Demaille and C. Taofifenua, *Phys. Chem. Chem. Phys.*, 2014, **16**, 4642-4652.
18. P. L. T. M. Frederix, P. D. Bosshart, T. Akiyama, M. Chami, M. R. Gullo, J. J. Blackstock, K. Dooleweerdt, N. F. d. Rooij, U. Staufer and A. Engel, *Nanotechnology*, 2008, **19**, 384004.
19. A. G. Güell, N. Ebejer, M. E. Snowden, J. V. Macpherson and P. R. Unwin, *J. Am. Chem. Soc.*, 2012, **134**, 7258-7261.
20. N. Ebejer, M. Schnippering, A. W. Colburn, M. A. Edwards and P. R. Unwin, *Anal. Chem.*, 2010, **82**, 9141-9145.
21. N. Ebejer, A. G. Güell, S. C. S. Lai, K. McKelvey, M. E. Snowden and P. R. Unwin, *Ann. Rev. Anal. Chem.*, 2013, **6**, 329-351.
22. B. D. B. Aaronson, C.-H. Chen, H. Li, M. T. M. Koper, S. C. S. Lai and P. R. Unwin, *J. Am. Chem. Soc.*, 2013, **135**, 3873-3880.
23. I. Heller, J. Kong, K. A. Williams, C. Dekker and S. G. Lemay, *J. Am. Chem. Soc.*, 2006, **128**, 7353-7359.
24. J. W. G. Wilder, L. C. Venema, A. G. Rinzler, R. E. Smalley and C. Dekker, *Nature*, 1998, **391**, 59-62.
25. A. G. Güell, K. E. Meadows, P. R. Unwin and J. V. Macpherson, *Phys. Chem. Chem. Phys.*, 2010, **12**, 10108-10114.
26. M. Berger, J. A. Gray and B. L. Roth, *Annual Review of Medicine*, 2009, **60**, 355-366.
27. P. Bertoncello, J. P. Edgeworth, J. V. Macpherson and P. R. Unwin, *J. Am. Chem. Soc.*, 2007, **129**, 10982-10983.
28. S. Sansuk, E. Bitziou, M. B. Joseph, J. A. Covington, M. G. Boutelle, P. R. Unwin and J. V. Macpherson, *Anal. Chem.*, 2012, **85**, 163-169.
29. A. N. Patel, P. R. Unwin and J. V. Macpherson, *Physical Chemistry Chemical Physics*, 2013, **15**, 18085-18092.
30. W. Harreither, R. Trouillon, P. Poulin, W. Neri, A. G. Ewing and G. Safina, *Anal. Chem.*, 2013, **85**, 7447-7453.
31. M. E. Snowden, A. G. Güell, S. C. S. Lai, K. McKelvey, N. Ebejer, M. A. O'Connell, A. W. Colburn and P. R. Unwin, *Anal. Chem.*, 2012, **84**, 2483-2491.
32. P. Hashemi, E. C. Dankoski, J. Petrovic, R. B. Keithley and R. M. Wightman, *Anal. Chem.*, 2009, **81**, 9462-9471.
33. M. Z. Wrona and G. Dryhurst, *Bioorganic Chemistry*, 1990, **18**, 291-317.

34. P. V. Dudin, M. E. Snowden, J. V. Macpherson and P. R. Unwin, *ACS Nano*, 2011, **5**, 10017-10025.
35. L. Huang, Z. Jia and S. O'Brien, *J. Mater. Chem.*, 2007, **17**, 3863-3874.
36. T. M. Day, N. R. Wilson and J. V. Macpherson, *J. Am. Chem. Soc.*, 2004, **126**, 16724-16725.
37. M. N. Szentirmay and C. R. Martin, *Anal. Chem.*, 1984, **56**, 1898-1902.
38. K. T. Rodolfa, A. Bruckbauer, D. J. Zhou, A. I. Schevchuk, Y. E. Korchev and D. Klenerman, *Nano Lett.*, 2006, **6**, 252-257.
39. Y. Wang, M. J. Kim, H. Shan, C. Kittrell, H. Fan, L. M. Ericson, W.-F. Hwang, S. Arepalli, R. H. Hauge and R. E. Smalley, *Nano Lett.*, 2005, **5**, 997-1002.
40. A. Reina, M. Hofmann, D. Zhu and J. Kong, *J. Phys. Chem. C*, 2007, **111**, 7292-7297.
41. S. Huang, X. Cai and J. Liu, *J. Am. Chem. Soc.*, 2003, **125**, 5636-5637.
42. S. J. Kang, C. Kocabas, T. Ozel, M. Shim, N. Pimparkar, M. A. Alam, S. V. Rotkin and J. A. Rogers, *Nature Nanotech.*, 2007, **2**, 230-236.
43. A. Rutkowska, D. Walker, S. Gorfman, P. A. Thomas and J. V. Macpherson, *J. Phys. Chem. C*, 2009, **113**, 17087-17096.
44. S. Huang, M. Woodson, R. Smalley and J. Liu, *Nano Lett.*, 2004, **4**, 1025-1028.
45. S. Huang, B. Maynor, X. Cai and J. Liu, *Adv. Mater.*, 2003, **15**, 1651-1655.
46. Z. Jin, H. Chu, J. Wang, J. Hong, W. Tan and Y. Li, *Nano Lett.*, 2007, **7**, 2073-2079.
47. R. Cui, Y. Zhang, J. Wang, W. Zhou and Y. Li, *J. Phys. Chem. C*, 2010, **114**, 15547-15552.
48. X. Wang, Q. Li, J. Xie, Z. Jin, J. Wang, Y. Li, K. Jiang and S. Fan, *Nano Lett.*, 2009, **9**, 3137-3141.
49. S. Li, Z. Yu, C. Rutherglen and P. J. Burke, *Nano Lett.*, 2004, **4**, 2003-2007.
50. B. H. Hong, J. Y. Lee, T. Beetz, Y. Zhu, P. Kim and K. S. Kim, *J. Am. Chem. Soc.*, 2005, **127**, 15336-15337.
51. A. Bezryadin, A. R. M. Verschueren, S. J. Tans and C. Dekker, *Phys. Rev. Lett.*, 1998, **80**, 4036-4039.
52. S. Heinze, J. Tersoff, R. Martel, V. Derycke, J. Appenzeller and P. Avouris, *Phys. Rev. Lett.*, 2002, **89**, 106801.
53. J. Kong, N. R. Franklin, C. Zhou, M. G. Chapline, S. Peng, K. Cho and H. Dai, *Science*, 2000, **287**, 622-625.
54. F. Léonard and J. Tersoff, *Phys. Rev. Lett.*, 2000, **84**, 4693-4696.
55. Z. Chen, J. Appenzeller, J. Knoch, Y.-m. Lin and P. Avouris, *Nano Lett.*, 2005, **5**, 1497-1502.
56. A. Javey, J. Guo, Q. Wang, M. Lundstrom and H. Dai, *Nature*, 2003, **424**, 654-657.
57. H. M. Manohara, E. W. Wong, E. Schlecht, B. D. Hunt and P. H. Siegel, *Nano Lett.*, 2005, **5**, 1469-1474.
58. M. Biercuk, S. Ilani, C. Marcus and P. McEuen, in *Carbon Nanotubes*, Springer Berlin Heidelberg, 2008, vol. 111, pp. 455-493.
59. M. S. Dresselhaus, G. Dresselhaus, R. Saito and A. Jorio, *Phys. Rep.*, 2005, **409**, 47-99.
60. A. Jorio, A. G. Souza Filho, G. Dresselhaus, M. S. Dresselhaus, A. K. Swan, M. S. Ünlü, B. B. Goldberg, M. A. Pimenta, J. H. Hafner, C. M. Lieber and R. Saito, *Phys. Rev. B*, 2002, **65**, 155412.
61. A. Jorio, R. Saito, J. H. Hafner, C. M. Lieber, M. Hunter, T. McClure, G. Dresselhaus and M. S. Dresselhaus, *Phys. Rev. Lett.*, 2001, **86**, 1118-1121.
62. S. D. M. Brown, A. Jorio, P. Corio, M. S. Dresselhaus, G. Dresselhaus, R. Saito and K. Kneipp, *Phys. Rev. B*, 2001, **63**, 155414.
63. T. S. Miller, N. Ebejer, A. G. Güell, J. V. Macpherson and P. R. Unwin, *Chem. Commun.*, 2012, **48**, 7435-7437.
64. Y. Fan, B. R. Goldsmith and P. G. Collins, *Nat. Mater.*, 2005, **4**, 906-911.